AIAA SciTech Forum
January 3-7, 2022, San Diego, CA & Virtual
AIAA SCITECH 2022 Forum

10.2514/6.2022-2222

A Reconfigurable Ducted Turbine Array Concept for Renewable Flow Energy Harvesting

Onur Bilgen,[*] Ruo-Qian Wang,[†] Yue Cao,[‡] Nazim Erol,[§] Xin Shan[**]

[*], [§], [**] *Department of Mechanical and Aerospace Engineering*
[†] *Department of Civil and Environmental Engineering*
Rutgers University, Piscataway, NJ 08854, USA

[‡] *School of Electrical Engineering and Computer Science*
Oregon State University, Corvallis, OR 97331, USA

This paper presents a reconfigurable ducted turbine array concept as a solution to reduce the cost of flow energy harvesting. The proposed distributed ducted direct-drive generator concept has a reconfigurable architecture to adjust to different flow conditions and various environmental and spatial constraints. The primary features, such as the ducted rotor, and the array configurations are presented. The paper focuses on the analysis of a single ducted turbine unit. A circular control volume is defined, and the flow distribution between the interior and the exterior of the duct is determined using an equivalent circuit analogy. Parametric analyses are conducted to understand the effects of a few key system parameters and design variables.

I. Introduction

Harvesting energy from fluid flows have been widely used in many applications including wind and hydrokinetic energy [1-3]. Particularly, hydrokinetic turbines have been utilized in hydroelectric power plants for decades. Hydrokinetic energy is a renewable energy resource with a considerable potential. The harvestable energy in tidal streams, ocean currents, and riverine currents is approximated at 2,051 TWh per year in the 50 states [4]. However, the utilization rate of hydrokinetic energy remains limited due to a high levelized cost of energy (LCOE.) The primary reason for the high cost is the challenges caused by the aquatic environment. Salinity, debris, strong marine flow, and various other factors bring difficulties to installing and maintaining hydrokinetic turbines. Also, hydrokinetic turbines work in a variety of environments, requiring a flexible design that can be reconfigured and optimized for different flow conditions.

A. Motivating Factors

Large structures are difficult to manufacture, install, operate, maintain, and decommission. Manufacturing is limited by machine tolerance limitations, and the total number of systems, and parts produced. Installation is limited by the weight of the system, which is typically proportional to the square of the characteristic length for shell-like thin-walled structures. Operation, maintenance, and decommissioning of large structures require large machines;

[*] Associate Professor, Mechanical and Aerospace Engineering, Rutgers University, AIAA Member.
[†] Assistant Professor, Civil and Environmental Engineering, Rutgers University.
[‡] Assistant Professor, School of Electrical Engineering and Computer Science, Oregon State University.
[§] Ph.D. Candidate and Graduate Research Assistant, Mechanical and Aerospace Engineering, Rutgers University.
[**] Ph.D. Candidate and Graduate Research Assistant, Mechanical and Aerospace Engineering, Rutgers University.

hence, lifetime costs can be prohibitively expensive for many applications. In contrast, small systems and components, produced in large numbers, can be assembled to produce the same level of useful work with much lower costs. Such low-cost systems can be easily scaled up or down to work for many applications. The need for large infrastructures, machines, and specialized equipment can be reduced or completely eliminated. There are many types of hydrokinetic devices that can produce energy from tidal and wave source without dam and penstock [5].

Duct augmentation can achieve higher power coefficient than the Betz Limit [6-8]. Diffuser augmentation to the duct design can increase the power coefficient as well [8, 9]. Most turbines/generators are non-direct-drive. They require a gearbox to increase the rotational speed to the generator. The reason for this comes for the basic principles of electromagnetic transduction. In an electromagnetic generator, voltage is related to the number of winding turns and rotor speed, and the current is related to the winding wire sizing, and power is the product of voltage and current. In a generator, geometrical laws/principles and structural/thermal/mass limitations do not allow for simultaneous maximization of the number of windings and the wire diameter. For an efficient operation, it is desirable to increase power by increasing voltage, rather than increasing current (e.g., resistive losses.) To increase voltage output, velocity (i.e., rotor speed, or rotor radius) must be increased. Introduction of a contracting duct can help increase rotor speed.

B. Contributions

A reconfigurable ducted turbine array concept is proposed to overcome the challenges listed above. The so-called macro unit is an assembly of many "identical" micro units (i.e., ducted turbines). The concept of distributing harvesting across multiple identical units is intended to reduce manufacturing, installation, and maintenance costs. Important features of the turbine array concept to improve the robustness and reduce the levelized cost of hydrokinetic energy is illustrated. In this paper, a single ducted turbine is parametrically analyzed. The primary design variables considered in this paper are the contraction ratio of the duct and the hub-to-throat radius ratio. Important response metrics such as duct mass, flow rates, and the available power are investigated as a function of design variables.

C. Outline

This paper will first introduce the conceptual design of a reconfigurable ducted turbine array. Next, the control volume and equivalent circuit modeling are presented. Then, a parametric analysis is conducted to understand the effects of design variables. Finally, conclusions are drawn.

II. The Reconfigurable Ducted Turbine Array Concept

The concept of reconfigurable ducted turbine array is a low-cost solution with flexibility to adapt to various flow conditions, potentially for both hydrodynamic and wind energy harvesting. The multi-layered micro-macro-farm architecture of turbine array enables multi-level and multi-scale modeling and optimization. Direct-drive generation is potentially used in the turbines, with mechanical simplicity and elimination of a large number of prismatic and revolute joints, gearbox, gearbox oil, and environmental contamination.

An assembly (i.e., array) of "micro" turbines creates a single macro turbine unit as shown in Figure 1. This feature allows for the same micro turbine unit to be assembled into an array that is specifically optimized for the application and location. The array can be rectilinear, radial, or any other geometry. Such array/assembly can be part of a turbine "farm" as it is done with conventional turbines today. Potential design variables for the macro unit include array arrangement (e.g., rectangular, circular, etc.), array size (N × M), and various other variables.

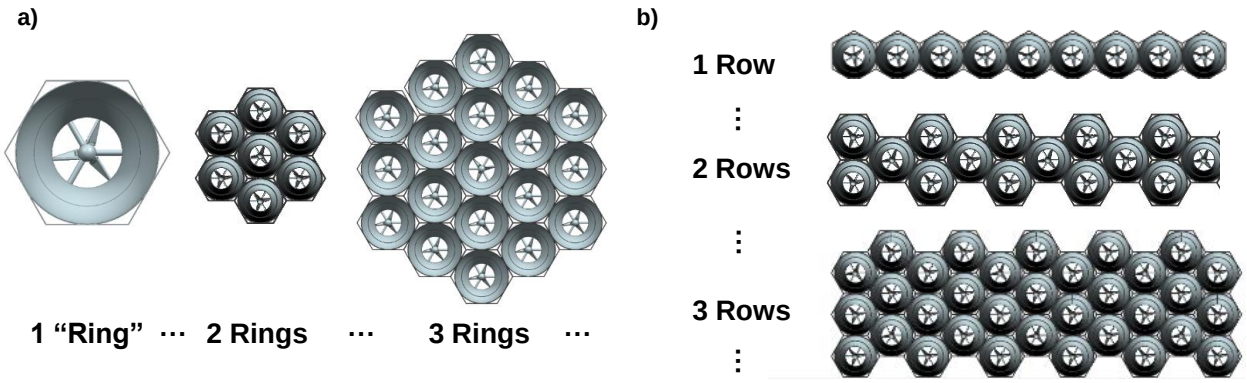

Figure 1: The reconfigurable ducted turbine array concept. Example a) circular, and b) rectangular array configurations.

The micro turbine is fully modular, and can be thought of a single "cube," "pixel," or a "cell" in a large assembly. A potential configuration consists of hexagonal cells, similar to cells in a honeycomb. A cell houses a turbine, potentially ducted. The duct (and the cell housing) provides the structure for the turbine, protects the rotor, and allows the turbine to be assembled into an array.

The proposed ducting is an important feature as it is not only of structural importance, but also has benefits for fluid flow conditioning, and for increasing power generation. First, the duct serves to reduce rotor blade tip vortex, which is a primary cause of inefficiency in nearly all rotating machinery that interacts with a fluid. Furthermore, the duct can be a contracting and expanding channel, similar to a wind or water tunnel. Low velocity at the inlet will accelerate within the contracting section to a higher velocity at the rotor section. This in return can cause the rotor to spin faster. A generator connected to the rotor would also rotate faster; hence, produce higher voltage and frequency, as desired by the power conversion electronics downstream. In most existing turbine applications, a gearbox is added to increase the speed to the generator such that voltage can be increased, while maintain the current at a manageable level, to maximize the power output. The ducting feature creates a potential to utilize a direct drive generator, eliminating the gearbox. The rotor velocity can be increased by increasing the flow velocity, rather than by using a gearbox.

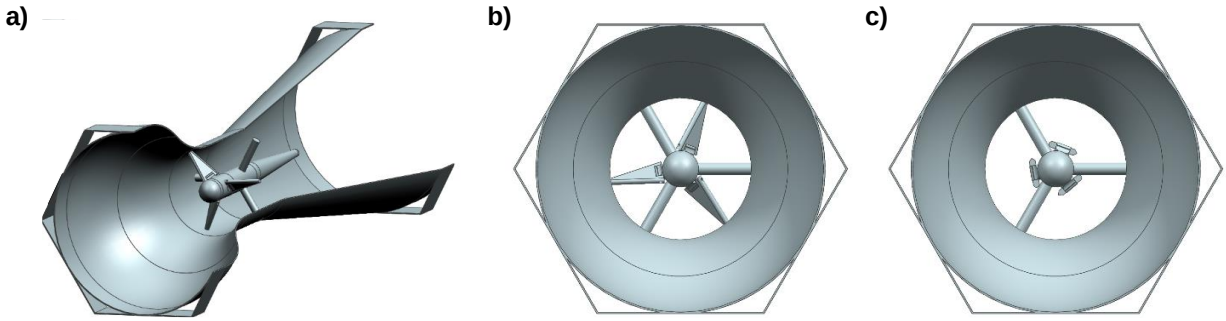

Figure 2: An example illustration of a single turbine "micro" unit. a) An example ducted direct-drive turbine. Downstream view with b) operating and c) folded blades in to the page. Blade geometry is for illustrative purposes only.

The rotor can have pitch and "coning" degrees-of-freedom for power optimization and system protection. For example, the coning control can be used to fold the blades for dislodging entanglement by opening the rotor plane as shown in Figure 2(c). Pitching and coning DOFs can be used to optimize power output, although mechanisms enabling these DOFs must be simple to reduce the cost.

A. Primary Features

The reconfigurable ducted turbine array has a multi-scale system architecture, i.e., farm-macro-micro levels. The assembly of the reconfigurable modular units is adaptable to various flow conditions. The flexible architecture with a large number of design variables allows pre-installation design optimization, adapting configuration for different applications and site geographies. Secondary (post-installation) or periodic design re-optimization is potentially allowed. The array can be reconfigured after an annual cycle.

The turbines can be in-situ continuous (on-demand) optimized for different power states, such as maximum power efficiency, maximum power output, maximum absolute lifetime, minimum operational variation between micro-units, and other desirable operational or non-operational states. It also supports smart on-demand maintenance as opposed to scheduled/periodic maintenance.

B. Application to Hydrokinetic Energy Harvesting

Figure 3 shows two applications of reconfigurable ducted turbine arrays adapting to different flow conditions. Figure 3(a) shows a potential application to riverine currents with uni-directional flow. In this application, arrays are deployed and installed on the riverbed. Figure 3(b) shows a potential application to tidal currents with bi-directional flow. For tidal flows, the system is moored and buoyant, and an anchoring system is required.

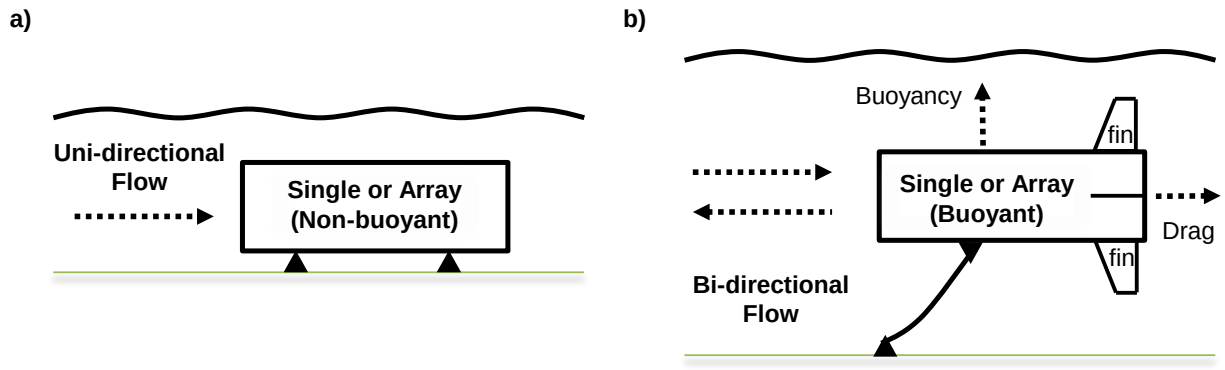

Figure 3: The reconfigurable ducted turbine arrays in: a) riverine uni-directional currents, and b) tidal bi-directional currents.

To reduce manufacturing and transportation costs, a limited number of standard micro units should be designed and manufactured, for example, a "small" unit, and a "large" unit. A standard shipping container, or a semi-truck trailer, is approximately 100 inches wide. Here, we propose a large turbine unit with inlet size of 96 inches (~2m). We also propose a small inlet size of 48 inches (~1m). Figure 4 presents various potential applications for the ducted array generators. Figure 4 (a-b) shows application to riverine uni-directional currents. Figure 4(c-d) shows application to tidal bi-directional currents.

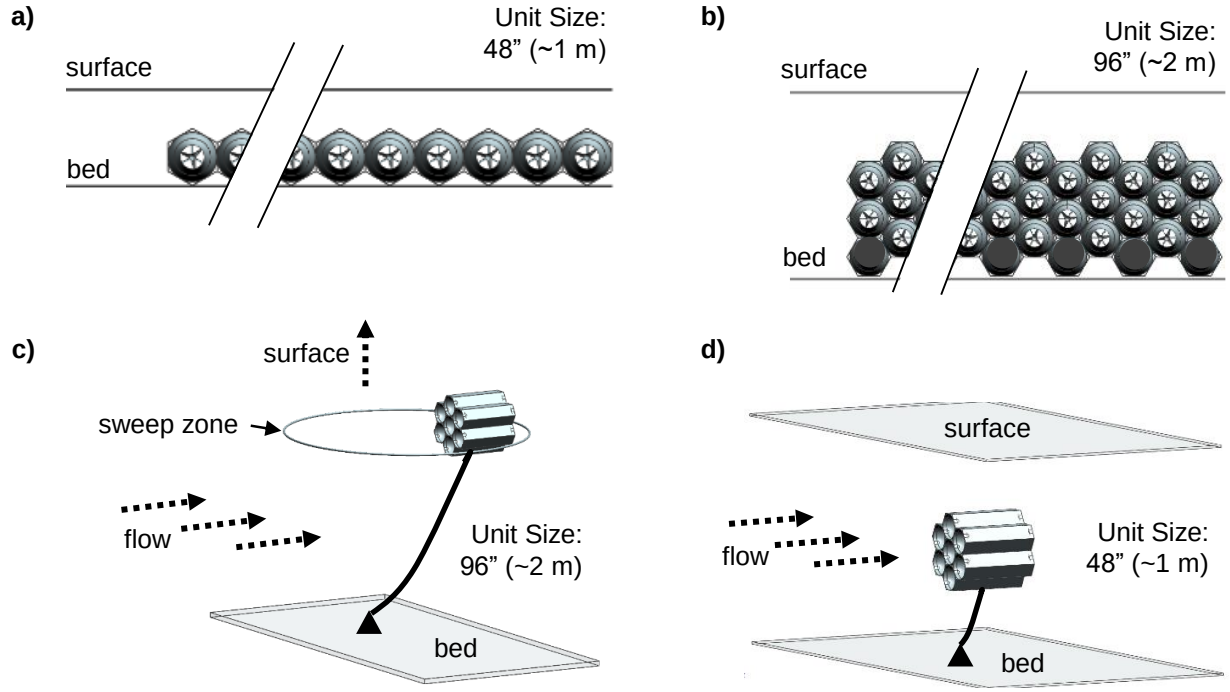

Figure 4: Applications for ducted array generators. Riverine uni-directional currents: a) Shallow river, b) deep river. Tidal bi-directional currents: c) deep waters, and d) shallow waters.

C. Parametrization of a Single Turbine

Important design variables are the aspect ratio, contraction ratio, critical angle, divergence angle, hub radius ratio, outlet-to-inlet radius ratio, and the inlet radius of the turbine. Some of the design variables are illustrated in Figure 5. The so-called contraction ratio, CR, is defined as the ratio of duct inlet diameter over the throat diameter. The contraction ratio greater than one can help to achieve larger velocity at the turbine area; however, this happens at the expense of a higher duct flow resistance and pressure drop. The so-called contraction region can be expanding instead, yielding a CR less than one. Hub radius ratio, HR, is defined as the throat diameter over the hub diameter. Hub ratio parameter is important because it defines a baseline for the electric generator to be used as well as contributing to the

resistance of the duct in turbine area. Thus, choosing the hub ratio is crucial for both accommodating the generator, as well as for reducing the resistance contributed by the hub. The outlet-to-inlet radius ratio, RR, is also defined. For ease of manufacturing and assembly, this ratio can be one; however, for hydrodynamic reasons, the outlet may be larger than the inlet. The so-called divergence angle, DA, is the angle at which section after the rotor expands. The divergence area is important to reduce separation/cavitation and pressure drop. Depending on other parameters, the "diverging" section can instead have a contracting shape. The critical angle is the largest angle of the duct profile in the contracting area. Finally, aspect ratio, AR, is defined as the ratio of overall duct length over the turbine inlet diameter. To reduce transportation costs, and overall mass, it is important to minimize the aspect ratio.

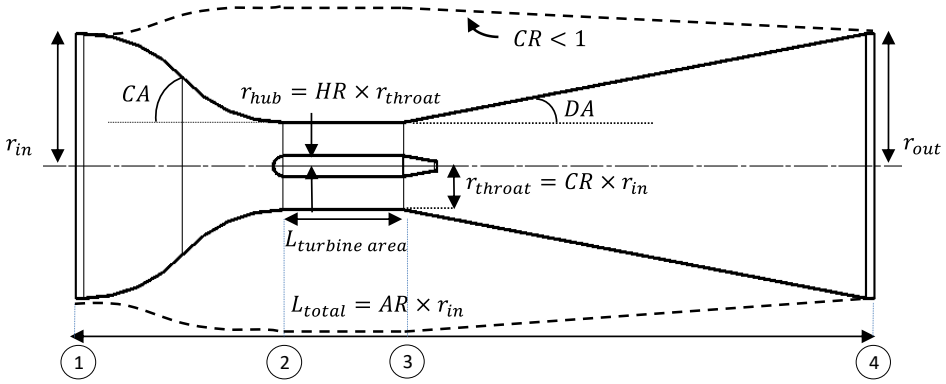

Figure 5: Illustration of some of the design variables on an example contracting-expanding ducted turbine with equal inlet and outlet radii. Dimensions are for illustrative purposes only.

A list of duct design variables and potential values are presented in Table 1.

Table 1: Some of the design variables for a single ducted turbine unit.

Design Variable		Example Values
$\boldsymbol{AR}$	Aspect Ratio	$0.1 - 4$
$\boldsymbol{CR}$	Contraction Ratio	$0.5 - 4$
$\boldsymbol{CA}$	Critical Angle	$\pm\ 0° - 45°$
$\boldsymbol{DA}$	Divergence Angle	$\pm\ 0° - 15°$
$\boldsymbol{HR}$	Hub-to-Throat Diameter Ratio	$0 \sim 1$
$\boldsymbol{d_{in}}$	Inlet Diameter	48", 96", etc.
$\boldsymbol{d_{out}}$	Outlet Diameter	24", 48", 96", etc.
$\boldsymbol{RR}$	Outlet-to-Inlet Diameter Ratio	$0.25 - 4$

A fully parameterized ducted turbine geometry model is generated using Siemens NX. Design variables are stored as expressions in Siemens NX. For this specific data collection, accessing and automating the response of the parameters were achieved using NX Open Python API, which allows user to automate processes in a code environment. Examples of effects of design variables are presented in Figure 6.

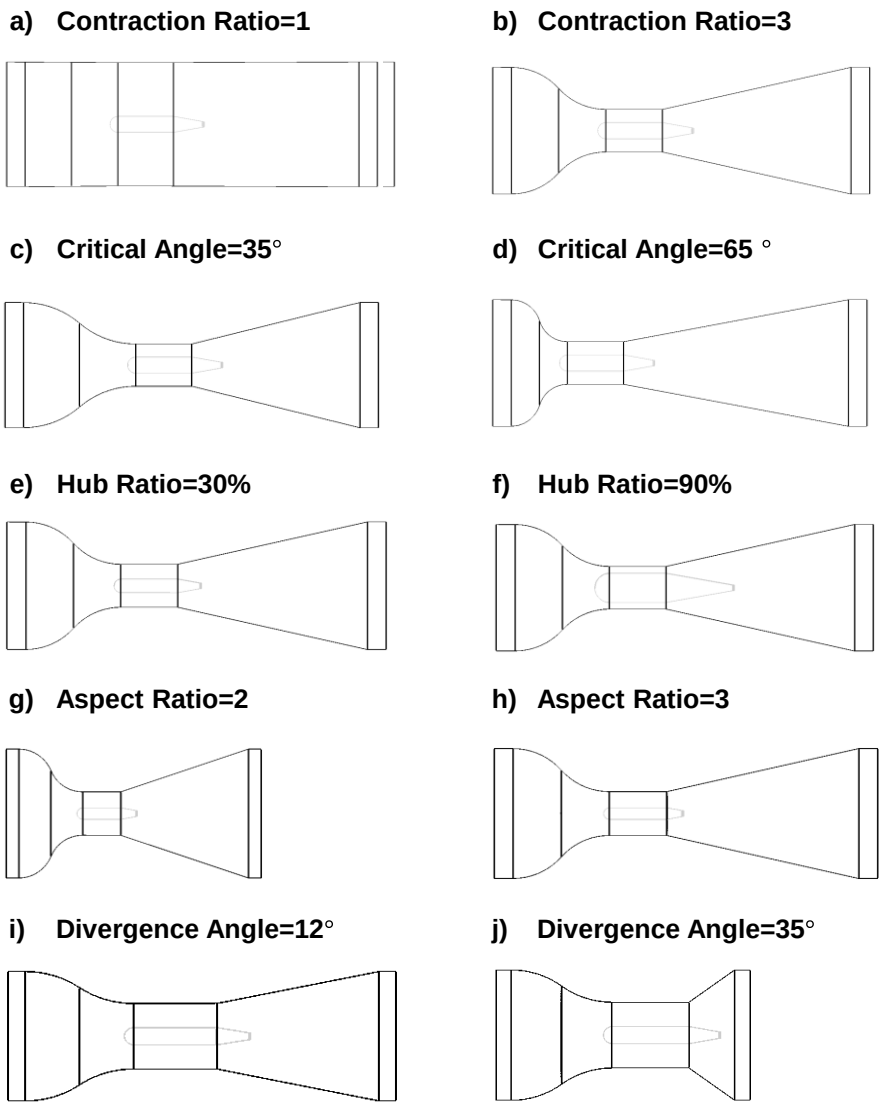

Figure 6. Examples of the effects of some of the design variables.

III. Modeling

A. Control Volume Definition

The control volume for our system is chosen to be circular because of its axisymmetric property. The control volume starts from station (0) with pre-defined velocity and pressure. Fluid density is assumed constant throughout. The control volume includes the duct and the turbine hub. Rotor is not included in this paper, although its effect will be represented by an equivalent blockage in the future. The duct system presented in Figure 7 consists of three segments: "contraction" area (1-2), turbine area (i.e., throat) (2-3), and the "divergence" area (i.e., diffuser) (3-4).

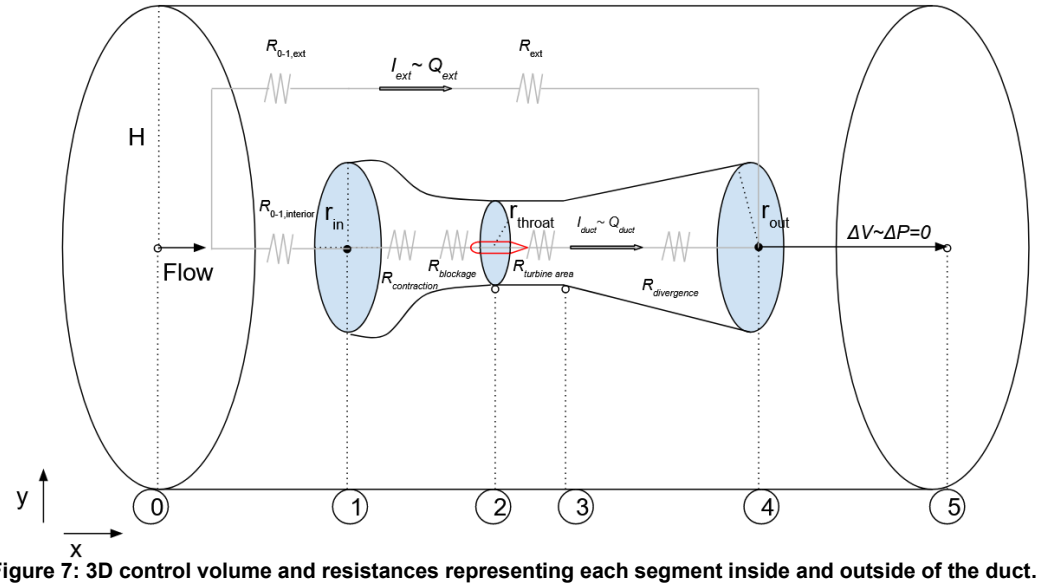

Figure 7: 3D control volume and resistances representing each segment inside and outside of the duct.

The key assumptions for the control volume are: 1) walls are fixed, 2) no-slip boundary conditions are applied, and 3) the duct is close to the riverbed. The duct is assumed to have a shell surrounding it from the inlet to the exit, so the annular exterior flow rate is calculated with constant inner radius rather than following the external profile of the duct. Flow entering the control volume will go through the inside of the duct as well as outside of the duct.

B. Equivalent Circuit Analysis and Flow Assumptions

In this paper, an equivalent electrical circuit analysis is utilized to estimate the flow behavior in terms of resistances and flow rate values. Various assumptions are made to simplify the analyses. The working fluid is assumed to be water. The flow is assumed to be fully laminar. It is known that the flow will be at least partially turbulent, particularly after it interacts with the rotor. In this paper, laminar analysis is used to determine maximum power available in an "ideal" turbine. In addition, flow is assumed to be incompressible and steady. Finally, the effect of gravity and the variation of hydrostatic pressure is ignored; however, gravity will be a key driver particularly for ducted turbines in riverine applications.

The equivalent circuit consists of two branches as illustrated in Figure 8. The top and bottom branches represent the exterior flow and the flow passing through the duct, respectively. The top branch has two resistors in series, i.e., the exterior resistance $R_{01,ext}$ before duct inlet, and the duct exterior resistance, R_{ext}. The bottom branch includes five resistances. The $R_{01,interior}$ is the interior resistance before the duct inlet, $R_{contraction}$ is due to the viscous resistance in the contraction region (1-2), $R_{blockage}$ is the resistance produced by the rotor. In this paper, $R_{blocakge}$ is assumed to be zero – an equivalent resistance as a function of rotor properties will be identified both theoretically and experimentally in the future. The $R_{turbine}$ and $R_{divergence}$ are the viscous resistances in segments (2-3) and (3-4) respectively. Note that the exterior and interior resistances before the duct, i.e., $R_{01,ext}$ and $R_{01,interior}$, account for the flow distribution due to the duct contraction, while the rest resistances are due to the viscous effects related to frictional energy loss.

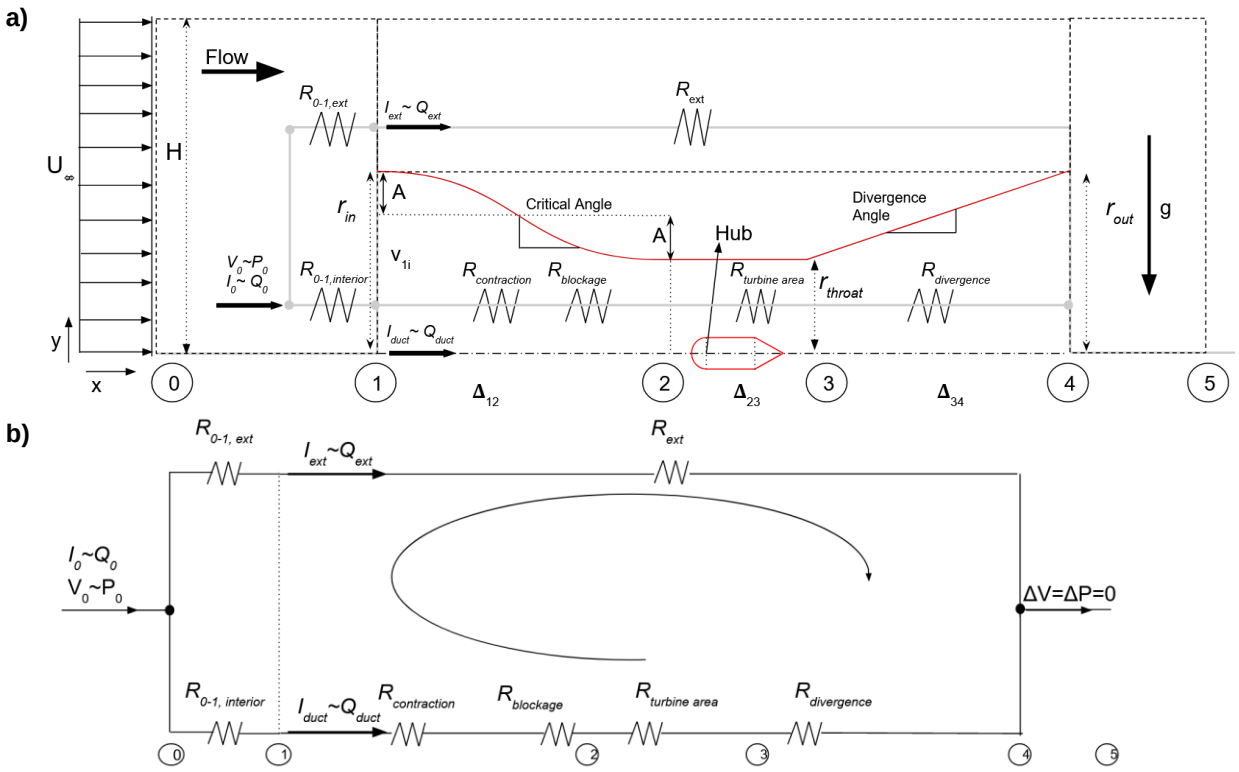

Figure 8: a) 2D control volume, and b) equivalent circuit diagram.

The resistance is calculated for each segment with varying lengths and radii. From circuit analogy, equivalent "mechanical" resistance is calculated using electrical resistance by:

$$R_{electrical} = \frac{\Delta V}{I} \text{ yielding } R = \frac{\Delta P}{Q}, \tag{1}$$

where the voltage, V, is analogous to pressure, P, and current, I, is analogous to flow rate, Q.

The resistances $R_{01,ext}$ and $R_{01,int}$ are assumed to have the following form:

$$\begin{aligned} R_{01,ext} &= C_1, \\ R_{01,int} &= C_1 \times f(CR) \frac{A_{ext}}{A_{throat}}, \end{aligned} \tag{2}$$

where A_{ext}/A_{throat} is the cross-section area ratio between the exterior of the duct and the interior (i.e. throat.) The exterior resistance (0-1) is assumed to be constant (C_1) for certain duct shell diameter and control volume, identified from numerical analysis or experiments. The factor $f(CR)$, which is a function of contraction ratio, and the area ratio are used to determine the $R_{01,int}$. When the contraction ratio is one, the factor $f(CR)$ converges to one. The flow inside and outside the duct becomes proportional to the area ratio.

The viscous resistance through a long cylindrical pipe with a constant cross-section is a function of its length and radius according to Poiseuille's Equation, which applies to a fully developed laminar flow [10]. This assumption can be adopted to analyze ducts with a high aspect ratio.

According to the Poiseuille's Equation, the flow rate in a circular pipe as a function of pressure is given by:

$$Q = \frac{\Delta P \pi r^4}{8 \mu \Delta x}, \tag{3}$$

where μ is the fluid viscosity, Δx is the segment length, and r is the radius throughout the duct. From Equations (1) and (3), we can re-write Poiseuille's Equation in terms of resistance by:

$$R_{circular} = \frac{\Delta P}{Q} = \frac{8\mu\Delta x}{\pi r^4}. \tag{4}$$

Resistances for the exterior region (1-4) and duct throat with hub (2-3) are annular sections, as shown in Figure 7. The resistance for an annular cross-section is given by [11]:

$$R_{annular} = \frac{1}{\frac{\pi {r_{outer}}^4}{8\mu\Delta x}\left[1 - \boldsymbol{r}^4 - \frac{(1-\boldsymbol{r}^2)^2}{-ln(\boldsymbol{r})}\right]} \tag{5}$$

where $\boldsymbol{r}$ is the radius ratio between the inner (r_{inner}) and outer (r_{outer}) radii of the annular cross-section. The ratio is limited between 0 and 1. In the case where $\boldsymbol{r} = 0$, the original Equation (4) is retrieved. In the case where $\boldsymbol{r} = \mathbf{1}$, resistance becomes infinite since the cross-section area vanishes.

As mentioned previously, there are two geometric configurations to compare. The baseline is a straight duct with constant diameter, and the other configuration is a "complex" duct with varying radii. Straight duct resistances are calculated by Equation (4) with a constant radius of the duct inlet. However, for the complex duct, the geometry is a function of position along the length of the duct, x.

Following are the radius definitions of the complex duct for each segment as shown in Figure 8a.

$$\begin{gathered} r_{12} = \frac{(r_{in} - r_{throat})}{2}\cos\left(\pi\frac{x}{\Delta_{12}}\right) + \frac{(r_{in} + r_{throat})}{2}, \\ r_{23,inner} = r_{hub} \quad \text{and } r_{23,outer} = r_{throat} \\ r_{34} = r_{throat} + \tan(\theta_{div})\, x. \end{gathered} \tag{6}$$

The total resistance for all of the segments of a long complex duct is given by:

$$R_{duct} = \int_0^{\Delta_{12}} \frac{8\mu}{\pi r_{12}(x)^4}\,dx + \frac{1}{\frac{\pi {r_{throat}}^4}{8\mu\Delta_{23}}\left[1 - (HR)^4 - \frac{(1-(HR)^2)^2}{-ln(HR)}\right]} + \int_0^{\Delta_{34}} \frac{8\mu}{\pi r_{34}(x)^4}\,dx + R_{blockage}, \tag{7}$$

where radiuses r_{ij} for each segment of the duct are given in Equation (6). The integration starts from 0 to the segment length. The exterior resistance, R_{ext}, is calculated by (5), where the inner radius is the inlet radius of the duct, r_{in}, and the outer radius is the control volume radius, H.

Kirchhoff's Voltage and Current Laws are essential for the derivation of the flow rates. To start off, Kirchhoff's Current law states that the sum of all currents entering and exiting a node must be zero.

$$\sum I_{in} - \sum I_{out} = 0 \tag{8}$$

For the node at location (0) in Figure 8, the current law yields the following flow rate relationship:

$$Q_0 = Q_{ext} + Q_{duct}, \tag{9}$$

which is the mass conversation. Additionally, Kirchhoff's voltage Law is applied in a closed loop where the sum of voltage changes must be zero.

$$\sum V = 0 = -V_{01,ext} - V_{ext} + V_{01,int} + V_{contraction} + V_{turbine\ area} + V_{blockage} + V_{divergence}, \tag{10}$$

which implies the assumption that the pressure drops at the top and bottom branches are identical. Rewriting in terms of resistance and flow rate, the following is obtained:

$$\begin{gathered} Q_{ext}\left(R_{01,ext} + R_{ext}\right) = Q_{duct}\left(R_{01,int} + R_{contraction} + R_{turbine\ area} + R_{blockage} + R_{divergence}\right), \\ Q_{ext}\left(R_{01,ext} + R_{ext}\right) = Q_{duct}\left(R_{01,int} + R_{duct}\right) \end{gathered} \tag{11}$$

Since we have two equations, (9) and (11), and two unknowns (Q_{ext} and Q_{duct}), the system of equations in matrix form is given by:

$$\begin{bmatrix} 1 & 1 \\ R_{01,ext} + R_{ext} & -(R_{01,int} + R_{duct}) \end{bmatrix} \begin{bmatrix} Q_{ext} \\ Q_{duct} \end{bmatrix} = \begin{bmatrix} Q_0 \\ 0 \end{bmatrix}. \quad (12)$$

From Equation (12), one can obtain values for the flow rates in the exterior and duct by:

$$\begin{bmatrix} Q_{ext} \\ Q_{duct} \end{bmatrix} = \begin{bmatrix} 1 & 1 \\ R_{01,ext} + R_{ext} & -(R_{01,int} + R_{duct}) \end{bmatrix}^{-1} \begin{bmatrix} Q_0 \\ 0 \end{bmatrix} \quad (13)$$

which is explicit since the resistances are independent of the flow rates.

IV. Parametric Analysis

A. Parameters and Responses

The flow in the proposed control volume is analyzed using the equivalent the circuit model presented above. Two separate duct shapes are analyzed: one is straight duct as a baseline, and the other is a so-called "complex" duct with varying radius along its length due to the design variables presented previously. Both of these shapes are considered without the gravity effect.

Independent Design Variables

The primary independent variables assumed for the parametric analysis are the contraction ratio and the hub ratio.

Constant (Assumed) Design Variables

The inlet and outlet radii are assumed to be 1 m. The turbine area (2-3) is 20% of the total length, and the divergence area (3-4) is 60% of the total length, and the remaining 20% is the contraction area (1-2). The aspect ratio, AR, is assumed to be six.

Dependent Design Variables

Critical angle, CA, and divergence angle, DA, are derived from the independent variables, and the constants assumed above.

Other Model Parameters:

The control volume inlet velocity, v_0, is assumed to be approximately 1.5 m/s. The control volume radius, H, is assumed to be 2 m.

Response Metrics

The following response metrics are observed: the flow rate and velocity at the rotor, duct mass, and the power available for extraction.

B. Duct Mass

The duct mass is analyzed for manufacturing, transportation and other factors that contribute to the overall cost of the system. For a straight duct with constant radius r, thickness t, length L, and density ρ, the mass is given by:

$$m = (2\pi r_{in} t L)\rho. \quad (14)$$

For a so-called "complex" duct with varying radius, the mass can be integrated by:

$$m = \left(\int_0^L 2\pi r(x) t dx \right) \rho. \quad (15)$$

where the radius profile function $r(x)$ is given in Equation (6). The mass of the duct as a function of contraction ratio is demonstrated in Figure 9. Mass of the complex duct is less than the straight duct because of the reduced surface area of the duct.

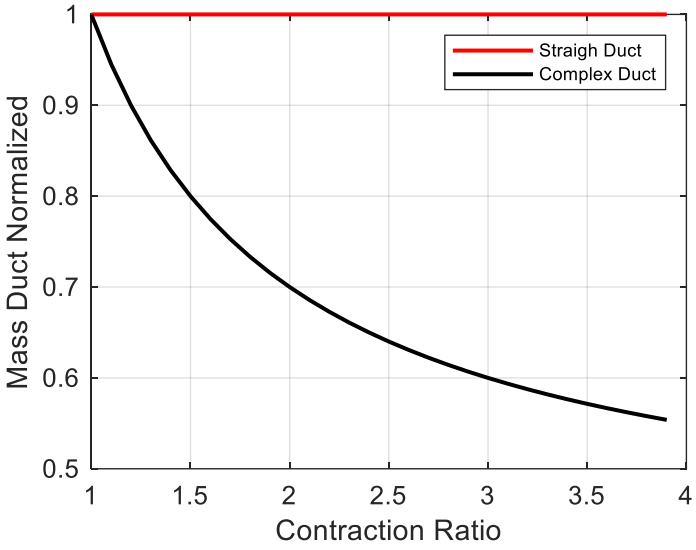

Figure 9: Mass of duct as a function of contraction ratio.

C. Velocity and Flow Rate

Velocity distribution is calculated from continuity. The control volume inlet flow rate Q_0 is calculated from the inlet velocity and diameter, which then exterior Q_{ext} and the duct Q_{duct} flow rates are calculated from Equation (13). At last, knowing the cross section area, A, velocities can be calculated from flow rates given by:

$$v = \frac{Q}{A}. \tag{16}$$

D. Fluid Power

The flow at the control volume inlet is shunted among the duct and exterior. This distribution is dictated by the blockage ratio, duct geometry, i.e., contraction and aspect ratio, etc., and duct flow resistance. The ratio of the energy entering the duct is denoted by the factor η_1. Inside the duct, the kinetic energy and pressure energy are exchanged as the cross-section area changes. Efficiency is calculated as a percentage of the available power out of the power entering the duct inlet. It is noted that the fluid power is not the same as "extractable" power.

Fluid energy at the i^{th} cross-section consists of the kinetic and "pressure" energies:

$$E_i = E_i^k + E_i^p = \frac{1}{2}\rho v_i^2 + P_i, \tag{17}$$

where E_i^k and E_i^p represent the kinetic and pressure energies respectively. The kinetic energy is calculated by the continuity relation (Equation (16)):

$$E_i^k = \frac{1}{2}\rho v_i^2 = \frac{1}{2}\rho\left(\frac{Q_{duct}}{A_1}\right)^2. \tag{18}$$

The Bernoulli's equation is used to obtain the pressure energy. The Bernoulli's equation from the duct inlet to the cross-section of interest is:

$$P_1 + \frac{1}{2}\rho v_1^2 - \Delta P_{1i} = P_i + \frac{1}{2}\rho v_i^2, \tag{19}$$

where pressure P_1 is the assumed absolute pressure at section 1 of the control volume, and ΔP_{1i} is the pressure loss from the duct inlet to the i^{th} cross-section due to flow resistance given by $Q_{duct} \times R_{1i}$. Substituting the continuity relation $v = Q/A$ in Equation (16), Equation (19) becomes:

$$P_i = P_1 + \frac{1}{2}\rho\left(\left(\frac{Q_{duct}}{A_1}\right)^2 - \left(\frac{Q_{duct}}{A_i}\right)^2\right) - \Delta P_{1i} \tag{20}$$

which gives the absolute pressure at different cross-sections of the duct. Next, the fluid power at the rotor location can be derived in terms of kinetic and pressure power.

$$Kinetic\ Power = \left(\frac{1}{2}\rho v_2^2\right) \times Q_{duct},$$
$$Pressure\ Power = P_2 \times Q_{duct}, \tag{21}$$
$$Total\ Power = \left(\frac{1}{2}\rho v_2^2 + P_2\right) \times Q_{duct}.$$

Lastly, power loss is calculated as:

$$Power\ Loss = \Delta P_{12} \times Q_{duct} \tag{22}$$

which is also applicable for other segments. The power available at each segment should be equal to the total power at the duct inlet minus the corresponding power loss.

V. Results

A. Ideal Flow

Equation (2) introduced resistances $R_{01,ext}$ and $R_{01,int}$ purely due to the contraction of the duct, accounting for the inviscid flow effects. These resistances can be identified from ideal flow simulations. The flow distribution between the duct interior and duct exterior is governed by the ratio of these two resistances. The $R_{01,int}$ is assumed constant as C_1 for a fixed control volume size and duct shell radius. This interior resistance $R_{01,ext}$, caused by the throat contraction, is proportional to the area ratio A_{ext}/A_{throat}. The fitting function $f(CR)$ in terms of contraction ratio is identified from ideal flow simulations. For straight duct, i.e., $CR = 1$, the function $f(CR)$ is one yielding a uniform flow.

The ideal flow simulations are conducted using the MATLAB PDE Toolbox by solving Laplacian equation for ideal flow. The fitting function $f(CR)$ in Equation (2) is identified by matching the flow rates and average velocities predicted by ideal flow simulations. The constant C_1 is arbitrary for ideal flow because it does not affect the ratio between interior and exterior flows. The constant C_1 becomes important to determine contributions from ideal flow and viscous effects in the circuit model, which will be identified later by viscous flow simulations.

The circuit model is identified using ideal flow simulations. Hub ratio is not considered in the ideal flow analysis. The viscosity is set to zero in the circuit model, thus leaving only ideal flow resistance in Equation (2). The identified model is given by:

$$R_{01,ext} = C_1,$$
$$R_{01,int} = C_1 \times f(CR)\frac{A_{ext}}{A_{throat}} = C_1 \times (1 - 0.38 \times log(CR)^{0.65})\frac{A_{ext}}{A_{throat}}. \tag{23}$$

The identified circuit model and the ideal flow model are compared with each other in Figure 10. Important response metrics of the system as a function of contraction ratio are presented. The flow rates are normalized with the total flow rate of the control volume. As expected, the summation of flow through duct and the flow through the exterior add up to 100% of the total flow rate.

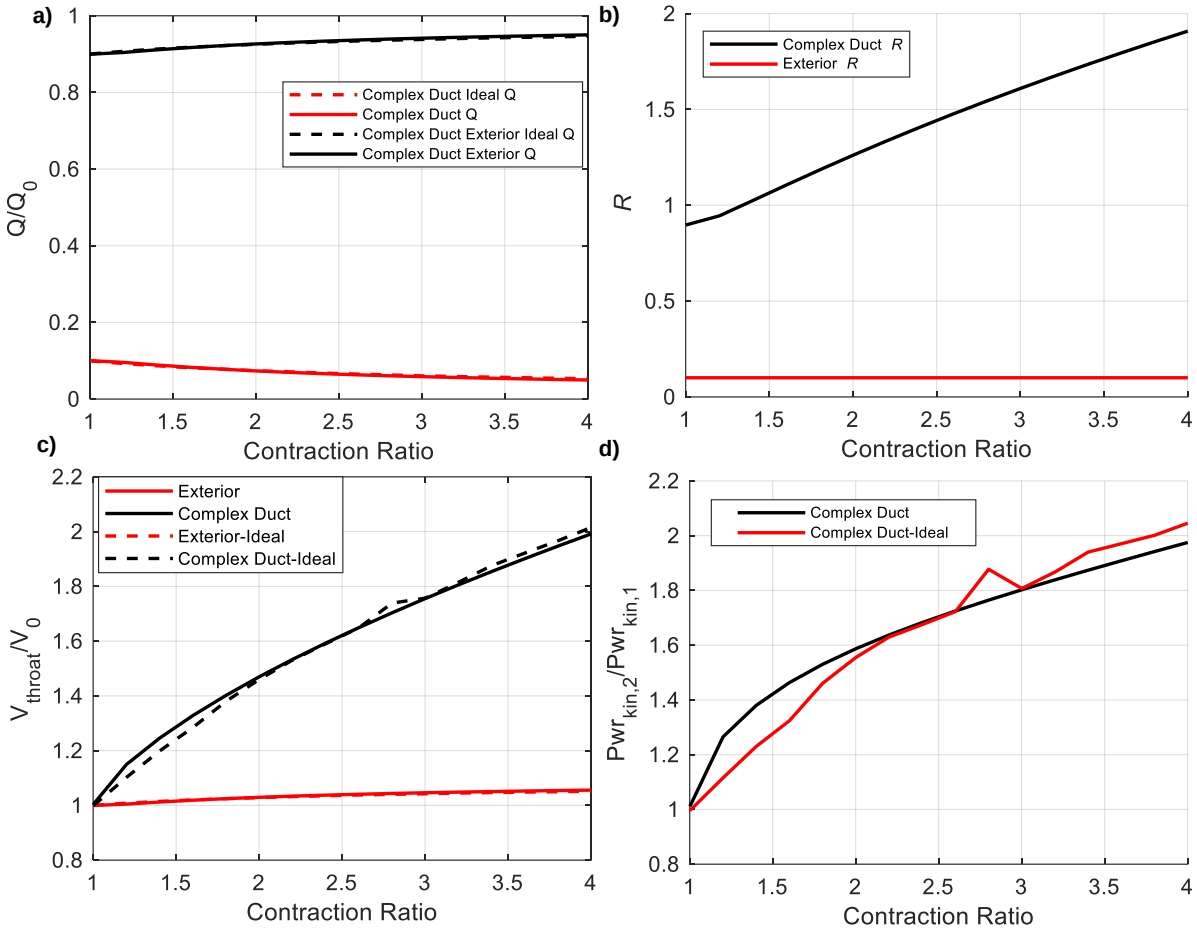

Figure 10: Response metrics as a function of contraction ratio. a) Flow Rate, b) resistance, c) velocity at throat, and d) kinetic power.

The resistance of the complex duct presented in Figure 10(b) increases as contraction increases whereas the resistance of the exterior region is constant C_1 because of the duct shell and control volume diameters do not change. Ideal flow velocities at the throat normalized by control volume inlet velocity are compared with circuit model velocities, the resemblance of the curves between the model and simulation are indeed in accordance with each other. Lastly, the normalized kinetic power in Figure 10(d) is also in accordance with each other.

B. Viscous Flow

When the duct is long, and accordingly the flow is fully developed in the duct, the viscous resistances predicted by Poiseuille's model in Equation (7) dominate the flow. In this section, only the viscous effects in the circuit model are studied without the ideal flow resistances in Equation (23). These results are purely to visualize flow results dictated by the wall friction. Figure 11 presents important response metrics of the system with changing contraction ratio. Each subplot shows two configurations: 1) straight duct, and the 2) complex duct. The flow rates are normalized with the total flow rate of the control volume as shown in Figure 11 (a). As expected, the summation of flow through duct and the flow through the exterior add up to 100% of the total flow rate. The resistance in the duct, shown in Figure 9(b), will be higher for a complex duct compared to a straight duct because of the contraction ratio reduces the throat radius. Another addition to the resistance is the hub ratio, and it creates an annular resistance. Figure 11 (c) presents the normalized velocity at the throat. Velocity at the throat should be much higher than straight duct; however, viscous resistance becomes the dominant which reduces the velocity in the contracted area. This is mainly to the assumptions that the duct is long, and the flow is fully developed. Another reason for this behavior is that the effect of gravity is ignored. Figure 11 (d) presents the kinetic power. Power available at the throat is normalized by the inlet duct power, and as the contraction ratio increases, the power reduces slightly.

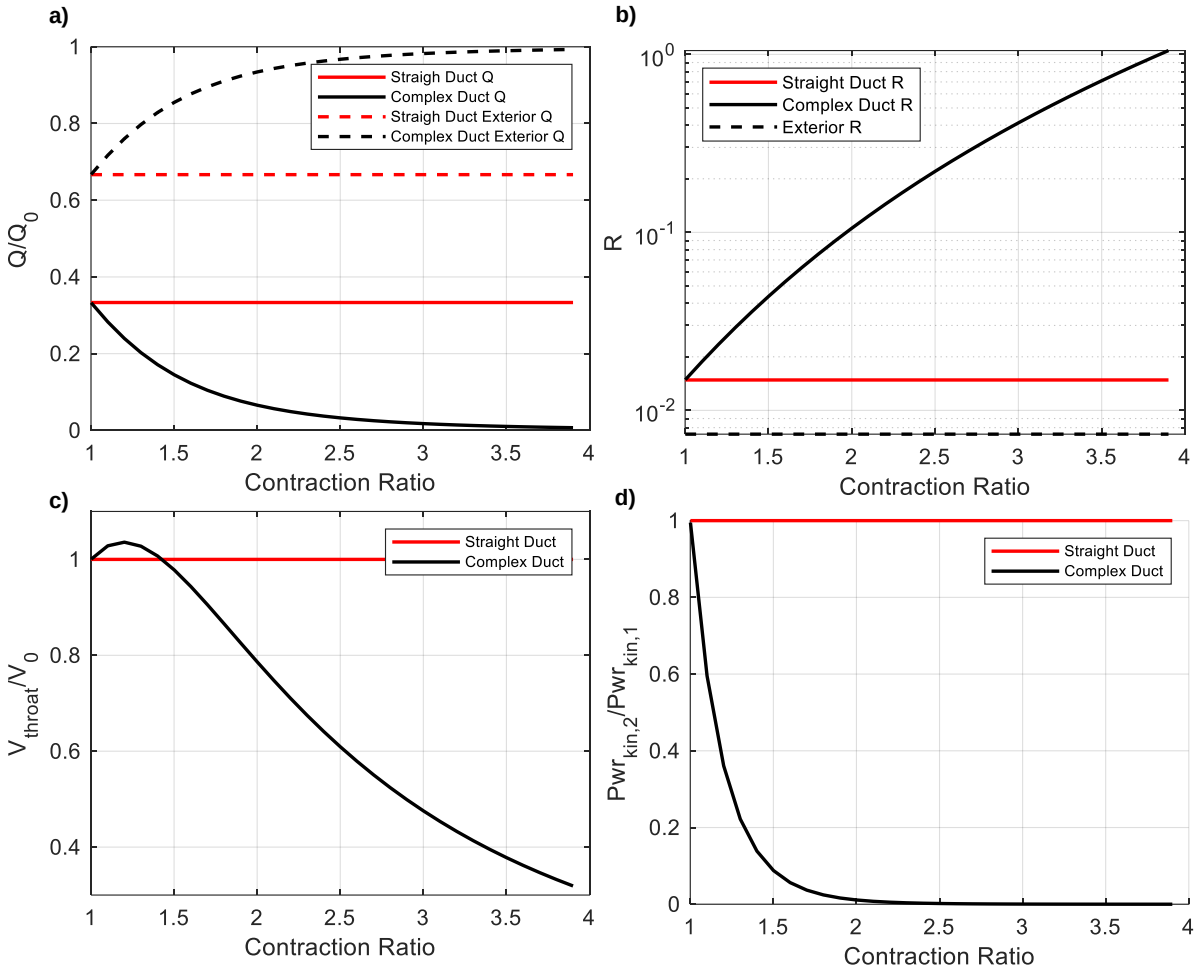

Figure 11. Response metrics as a function of contraction ratio. a) Flow through the duct, and flow through the exterior, b) resistance inside of the duct, c) the velocity at the turbine area, and d) normalized kinetic power.

In Figure 12, the hub ratio effect is demonstrated with a constant contraction ratio of two for the complex duct. Figure 12(a) presents the flow through the duct and the region exterior of the duct. The exterior and duct flow rates add up to 100% as expected. Figure 12(b) presents resistance as a function of hub radius ratio. Lastly, Figure 12(c) presents the normalized velocity at the throat.

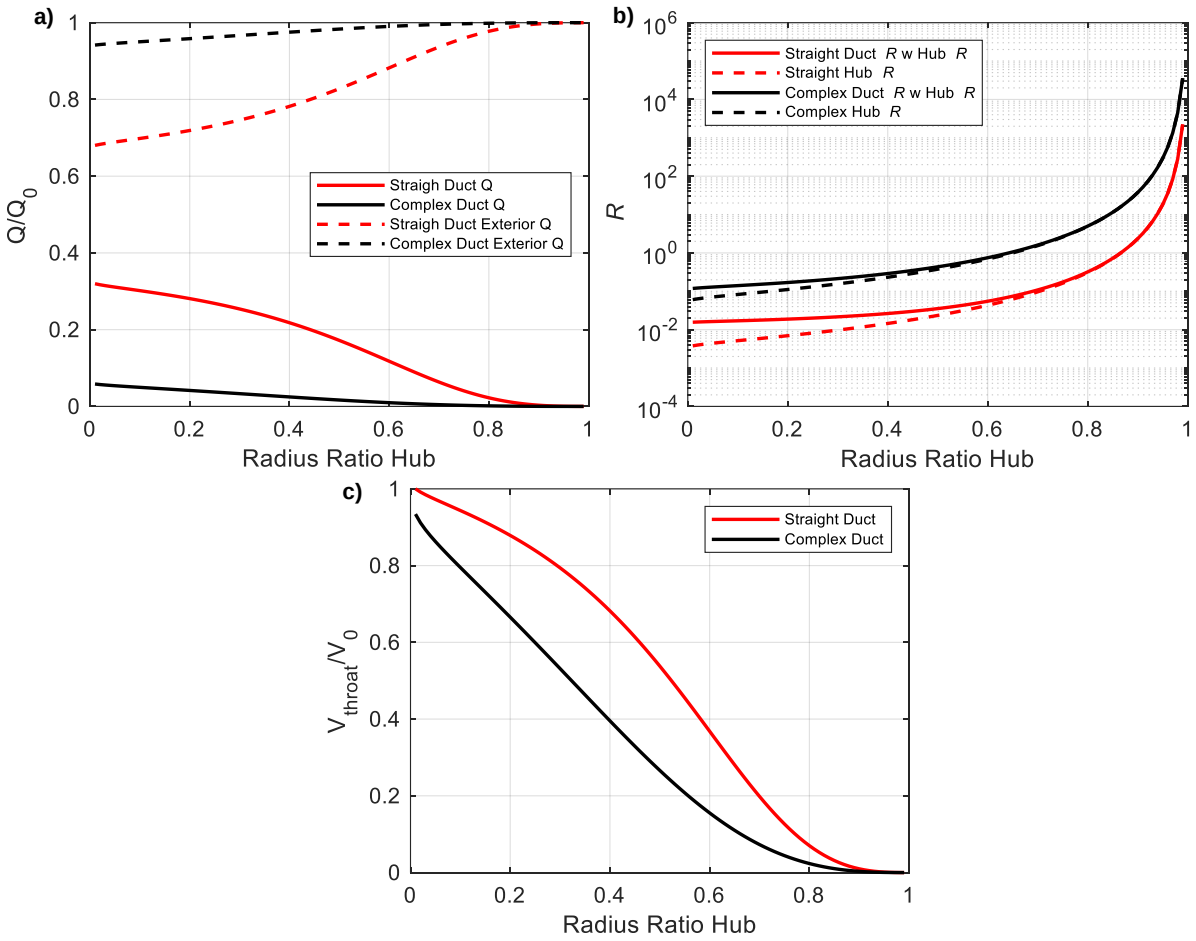

Figure 12: Important response metrics as a function of hub ratio. a) Flow through the duct, and flow through the exterior, b) resistance inside of the duct, and c) the velocity at the turbine area.

C. Ideal and Viscous Flow Combined

The results above are for the ideal flow case in Section A, where $f(CR)$ was identified, and for the viscous flow case in Section B based on Poiseuille's equation. In this section, both ideal flow and viscous effects are included in the circuit model given by Equation (12). The control volume is 2D for the ideal flow simulations. Hub ratio is not considered in the combined analysis.

The constant C_1 in Equation (23) represents the relative contributions from ideal flow effects, represented by $R_{01,ext}$ and $R_{01,int}$, and viscous effects, represented by the Poiseuille's equation in Equation (7). A higher C_1 leads to a flow field governed by ideal flow, while a lower C_1 indicates prominence of viscous effects. The revised circuit model is given by:

$$R_{01,ext} = C_1 = 0.185,$$
$$R_{01,int} = C_1 \times f(CR)\frac{A_{ext}}{A_{throat}} = 0.185 \times (1 - 0.38 \times log(CR)^{0.65})\frac{A_{ext}}{A_{throat}}. \quad (24)$$

The responses from the revised circuit model in Equation (24) and viscous flow simulations are presented in Figure 13. The flow rate results show very good agreement, where both duct and exterior flow rates add up to 100%. Circuit model resistances shown in Figure 13(b) increases in duct with contraction ratio, and is constant for the exterior section because duct and control volume diameter are constant. Normalized velocity shown in Figure 13(c) has peaks higher than free stream velocity from $CR{\sim}1.2-2$; however it drastically decreases due to contraction and increase in boundary friction and viscous effect. As seen after $CR{\sim}2$, the velocity for the ideal flow simulation is not smooth. The fluctuation is due to the laminar solution becoming unstable when higher contraction causes separation after the throat region. Thus, the ideal flow simulations are used for an appropriate contraction ratio range where the streamlines

are smooth and not disturbed (i.e. $CR = 1 - 2.5$.) The throat velocity Figure 13(c) and kinetic power Figure 13(d) are both slightly overestimated at low contraction ratios. The throat velocity is accelerated, and the kinetic power is enhanced by the appropriate contraction ratio.

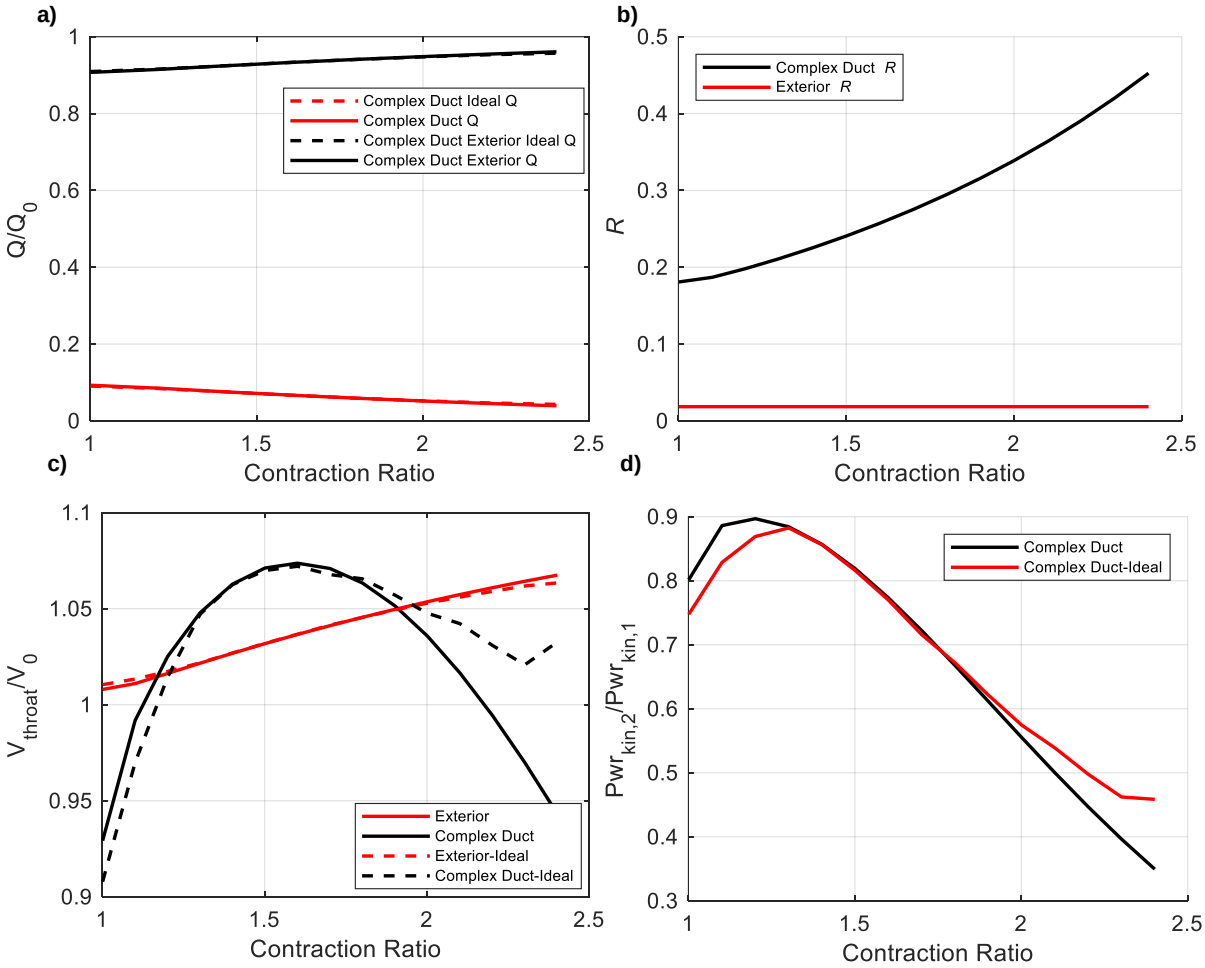

Figure 13: Important response metrics as a function of contraction ratio. a) Normalized flow rate, b) resistance, c) normalized throat velocity, and d) normalized kinetic power.

VI. Conclusions

This paper presents a reconfigurable ducted turbine array concept as a solution to reduce the levelized cost of flow energy harvesting. The concept of distributing harvesting across multiple identical units is intended to reduce manufacturing, installation, and maintenance costs. Important features of the turbine array concept to improve the robustness and reduce the levelized cost of hydrokinetic energy is illustrated. The turbine array is parametrically analyzed at the micro level. The design variables considered in this paper are hub ratio and contraction ratio for a single ducted turbine unit. The resistance model is adopted from circuit analogy to observe the behavior of the flow with different design variables.

Acknowledgments

The research presented in Sections III – V were partially supported by the U.S. Department of Energy (DOE) *Advanced Research Projects Agency-Energy* (ARPA-E) *Submarine Hydrokinetic and Riverine Kilo-megawatt Systems* (SHARKS) Program award number DE-AR0001438.

References

[1] O. Bilgen, J. G. Kenerson, M. Akpinar-Elci, R. Hattery, and L. M. J. T. J. o. C. H. Hanson, "The Search for High-Impact Diagnostic and Management Tools for Low-and Middle-Income Countries: A Self-Powered Low-Cost Blood Pressure Measurement Device Powered by a Solid-State Vibration Energy Harvester," vol. 17, no. 8, pp. 644-650, 2015.

[2] O. Bilgen, J. G. Kenerson, M. Akpinar-Elci, and R. Hattery, "Harvesting energy from internal flows with submerged piezocomposite transducers," in *24th AIAA/AHS Adaptive Structures Conference*, 2016, p. 1793.

[3] R. Hattery, O. J. S. s. Bilgen, and systems, "Harvesting energy from acoustic vibrations of conventional and ultrasonic whistles," vol. 19, no. 6, pp. 615-624, 2017.

[4] U. DOE, "Quadrennial Energy Review," ed: Washington, 2015.

[5] L. I. Lago, F. L. Ponta, and L. Chen, "Advances and trends in hydrokinetic turbine systems," *Energy for Sustainable Development*, vol. 14, no. 4, pp. 287-296, 2010.

[6] M. O. L. Hansen, N. N. Sørensen, R. J. W. E. A. I. J. f. P. Flay, and A. i. W. P. C. Technology, "Effect of placing a diffuser around a wind turbine," vol. 3, no. 4, pp. 207-213, 2000.

[7] B. Kirke, "Developments in ducted water current turbines," 2003, Art. no. 30249.

[8] K. M. Foreman, B. Gilbert, and R. A. Oman, "Diffuser augmentation of wind turbines," *Solar Energy*, vol. 20, no. 4, pp. 305-311, 1978/01/01/ 1978.

[9] B. Kosasih and H. Saleh Hudin, "Influence of inflow turbulence intensity on the performance of bare and diffuser-augmented micro wind turbine model," *Renewable Energy*, vol. 87, pp. 154-167, 2016.

[10] M. Zamir, *The Physics of Coronary Blood Flow*. Springer US, 2006, pp. 41-46.

[11] C. Kleinstreuer, *Modern fluid dynamics*. Springer, 2018, pp. 360-362.